Direct observation of frozen moments in the NiFe/FeMn exchange bias system

2013 New J. Phys. 15 033016

(http://iopscience.iop.org/1367-2630/15/3/033016)

New Journal of Physics
The open access journal for physics

Direct observation of frozen moments in the NiFe/FeMn exchange bias system

J Mohanty[1,2,6], A Persson[3,5], D Arvanitis[3], K Temst[4] and C Van Haesendonck[1]

[1] Laboratory of Solid-State Physics and Magnetism, KU Leuven, Celestijnenlaan 200D, BE-3001 Leuven, Belgium
[2] Indian Institute of Technology Hyderabad, Ordnance Factory Estate, Yeddumailaram, Andhra Pradesh 502205, India
[3] Physics Department, Uppsala University, Box 530, SE-75121 Uppsala, Sweden
[4] Instituut voor Kern- en Stralingsfysica, KU Leuven, Celestijnenlaan 200D, BE-3001 Leuven, Belgium
E-mail: jmohanty@iith.ac.in

New Journal of Physics **15** (2013) 033016 (10pp)
Received 23 July 2012
Published 12 March 2013
Online at http://www.njp.org/
doi:10.1088/1367-2630/15/3/033016

Abstract. We detect the presence of frozen magnetic moments in an exchange biased NiFe ferromagnet at the NiFe/FeMn ferromagnet/antiferromagnet interface by magnetic circular dichroism in x-ray absorption and resonant reflectivity experiments. Frozen moments are detected by means of the element-specific hysteresis loops. A weak dichroic absorption with unidirectional anisotropy can be linked to frozen magnetic moments in the ferromagnet. A more pronounced exchange bias for increasing the thickness of the FeMn layer correlates with an increase in orbital moment for interface Ni atoms carrying a frozen moment. These atoms compose about a single monolayer, but only a fraction of the atoms contributes by means of a strongly enhanced orbital moment to the macroscopic exchange bias phenomenon. The microscopic spin–orbit energy associated with these few interface frozen moment atoms appears to be sufficient to account for the macroscopic exchange bias energy.

[5] Current address: Outokumpu Stainless AB, Avesta Research Centre, Koppardalsvägen 65, PO Box 74, SE-774 22 Avesta, Sweden.
[6] Author to whom any correspondence should be addressed.

Exchange bias (EB) [1–3] is an interface coupling phenomenon in which a ferromagnet (FM) is magnetically coupled to an antiferromagnet (AFM) and the magnetization of the FM is pinned by the AFM along a particular direction, leading to a unidirectional shift of the hysteresis loop. This coupling phenomenon is used in magnetic high-density storage devices such as spin valves [4] and magnetic recording heads [5, 6]. It has been proposed that the EB effect originates from a small number of uncompensated interfacial spins located at the FM/AFM interface that do not follow the external field (frozen magnetic moments) [7–12]. Uncompensated spins associated with the AFM have been observed in several systems: in Co/FeMn [7], Co/IrMn [8] and Co/NiO [9] by using x-ray magnetic circular dichroism (XMCD), in Co/FeF_2 by using magnetic x-ray scattering and polarized neutron reflectivity [10], in CoO/NiFe by using SQUID magnetization measurements [12] and in CoO/CoPt multilayers by using magnetic force microscopy [13]. Experimental evidence for frozen magnetic moments has been reported for the systems Fe/FeF_2 and Fe/MnF_2 [14].

In this study, we rely on soft x-ray absorption spectroscopy (XAS) based on total electron yield (TEY) measurements for the detection of the XMCD, and on element-specific magnetic hysteresis (ESMH) loops taken in the x-ray resonant reflectivity (XRR) mode. Our EB system is $Ni_{80}Fe_{20}$(FM)/$Fe_{50}Mn_{50}$(AFM). In addition to the known XMCD signal associated with the bulk of the $Ni_{80}Fe_{20}$ FM layer, we measure a weak frozen moment Ni XMCD signal on the FM side of the FM/AFM interface for this EB system. This is a distinct Ni XMCD signal consistent with the unidirectional EB field symmetry. We measure the frozen moment Ni XMCD for varying layer thickness of the AFM and compare the results of these measurements to the measured ESMH loops. Surprisingly, we find that the frozen magnetic moments originate from Ni atoms located on the FM side of the FM/AFM interface, rather than on the AFM side as reported previously for the uncompensated spins [7–10, 12, 13]. We characterize the frozen Ni moments in terms of orbital and spin moments per atom. The ESMH loops allow us to probe deeper into the FM due to a different length scale that is being probed. The XMCD and XRR data indicate that there is about one monolayer of frozen magnetic moments on the FM side of the interface. Only a small fraction of these moments is found to carry an enhanced orbital moment, which appears to be at the origin of the EB effect. Our findings evidence the presence of both ‘passive’ and ‘active’ frozen magnetic moments at the FM/AFM interface.

Our Si(111)/Cu/NiFe/FeMn/Au samples are grown by molecular beam epitaxy in the presence of a magnetic field (≈10 mT) to initiate EB. For our study, we rely on three NiFe/FeMn (FeMn AFM on top) bilayer samples with a 5 nm NiFe thickness and different FeMn thicknesses: 7 nm (sample (a)), 9 nm (sample (b)) and 10 nm (sample (c)). On the other hand, we rely on two FeMn/NiFe bilayers (NiFe FM on top) with a 5 nm NiFe thickness and two different FeMn thicknesses: 7 nm (sample (d)) and 9 nm (sample (e)). Finally, we rely as well on two reference single NiFe FM layers having the same thickness of 5 nm and which we refer to as sample ‘reference’ and sample ‘reference 1’. These two samples were grown in different batches with the same deposition conditions. All samples have 1.5 nm of Au cap layer for oxidation protection. All samples were characterized by means of x-ray reflectivity and atomic force microscopy [15]. The x-ray reflectivity data indicate that the roughness of the layer interfaces of our samples is in the atomic layer range or less. The x-ray dichroism experiments were performed using the D1011 bending-magnet-based beamline at the synchrotron laboratory MAX-lab in Lund, Sweden. Beamline D1011 provides x-rays in the energy range between 30 and 1500 eV with a variable degree of circular polarization. We have set the degree of circular polarization to 0.85 for our measurements. The light helicity was kept constant. We use the

TEY mode to obtain the XAS and XMCD spectra. We also took data in the XRR mode both versus photon energy at fixed x-ray incidence angle and versus the incident angle at fixed photon energy to obtain ESMH loops. For the XRR-based measurements, we used an x-ray photodiode detector in the θ–2θ geometry, where the x-rays were incident at grazing angles (5–15°). The escape depth of the reflected photons along the normal to the surface is considerably larger than that for the electrons, despite the fact that we work under resonant conditions. We record here the electron yield, a quantity proportional to the absorption coefficient. The x-ray attenuation length in the spectral range used here for the samples we investigate can be calculated using both the measured spectra, obtained in arbitrary units, and the tabulated atomic cross sections in the photon energy range of interest once the materials elemental composition, eventual layer geometry and density are given [21]. The use of the tables allows obtaining the x-ray attenuation length in the high-energy non-resonant part of the spectra. This quantity can then be deduced for the whole spectral range measured, using the measured electron yield spectra. We estimate that for the FeMn we have to deal with a characteristic photon escape length of about 7 nm at the Fe L_3 edge, while for the NiFe we have to deal with an escape length of 4 nm at the Ni L_3 edge. On the other hand, for the XMCD experiment where electrons are detected, we probe the sample within a characteristic depth of only about 2 nm [22, 23].

The measuring geometries for our TEY XMCD measurements are presented in figure 1(c). For 'normal' XMCD measurements, we rely on geometries 1 and 2, where the circularly polarized x-rays are incident on the sample at an angle of 45° and the magnetic field is applied along the EB direction using a pair of Helmholtz coils. The direction of the applied homogeneous magnetic field is indicated by two sets of parallel arrows. For these normal XMCD measurements, we stay at 45° and apply a magnetic field, which exceeds the coercive field H_c for both the positive and negative field directions. After proper normalization and subtraction the corresponding XAS spectra yield the XMCD signal presented in figure 1(a) for sample (d) at the Ni L_3 edge. In this geometry no XMCD contribution is expected from the AFM part of the sample or the frozen moments, as we use moderate magnetic fields (up to 500 G) that only influence the ferromagnetic part of the sample.

Assuming that there exist frozen moments near the FM/AFM interface, which are related to the unidirectional EB field, another type of experiment needs to be performed to record the XMCD signal associated with these frozen moments (figure 1(b)). We used the so-called 'left'- and 'right'-handed geometries, where the sample is rotated from a +45° angle (figure 1(c), measurement geometry 3) toward a −45° angle (figure 1(c), measurement geometry 4). The latter measurement geometries are relevant since the frozen moments change then from parallel to anti-parallel with respect to the incident x-rays as one turns the sample from +45° to −45°. We, hence, take spectra with the EB field direction parallel as well as anti-parallel to the incident x-rays. The differences between these XAS spectra taken with the 'left'- and 'right'-handed geometries provide the frozen moments that do not respond to the applied magnetic field. It should be noted that the EB direction defines the direction of the frozen moments. We have attempted XMCD measurements at the Mn L-edges without detecting any XMCD signal. This is not surprising as FeMn is an AFM. A dichroic signal would be detected in an XMLD geometry, an experiment we do not report here.

For measuring the ESMH loops we also rely on the 'left'- and 'right'-handed measurement geometries presented in figure 1(c) (panels 3 and 4), but now at grazing incidence angles of the x-rays. For XRR at a fixed photon energy, we present in figure 2 loops taken at + and −7° grazing incidence angles.

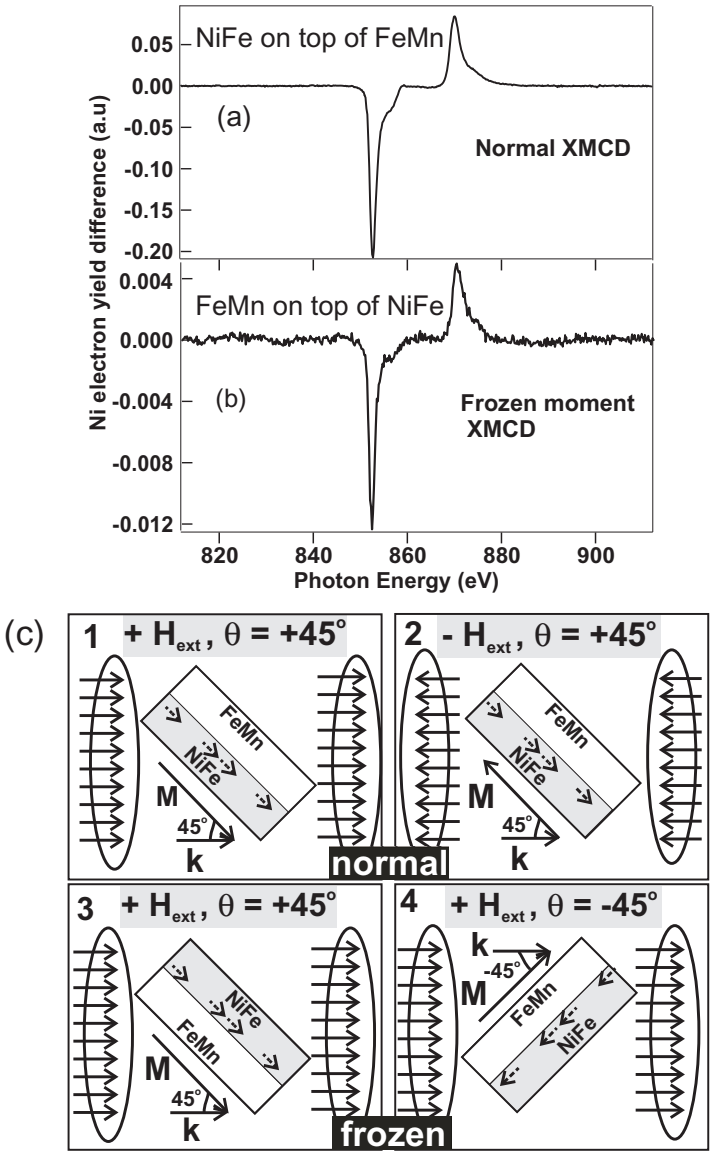

Figure 1. (a) The 'normal' Ni XMCD spectrum for a FeMn/NiFe bilayer (NiFe on top, sample (d)) and (b) the XMCD Ni spectrum associated with frozen Ni magnetic moments for a NiFe/FeMn sample (FeMn on top, sample (a)). In (c), we schematically present the measuring geometries used to determine the normal spectrum (1 and 2) and the spectrum associated with the frozen moments (3 and 4). The incident x-ray direction is denoted by the k-vector; the x-rays are incident at an angle of 45° with respect to the sample surface. Parallel arrows indicate the direction of the applied field, and M denotes the orientation of the magnetization within the FM that is imposed by the applied field. Interface frozen moments are schematically illustrated by dotted arrows.

Together with the shift in H_c, we clearly observe a vertical shift of the loops when comparing the 'right-handed' to the 'left-handed' geometries. This indicates the presence of frozen moments at the interface for both sample (a) and sample (b) [11, 16–18]. Both loops

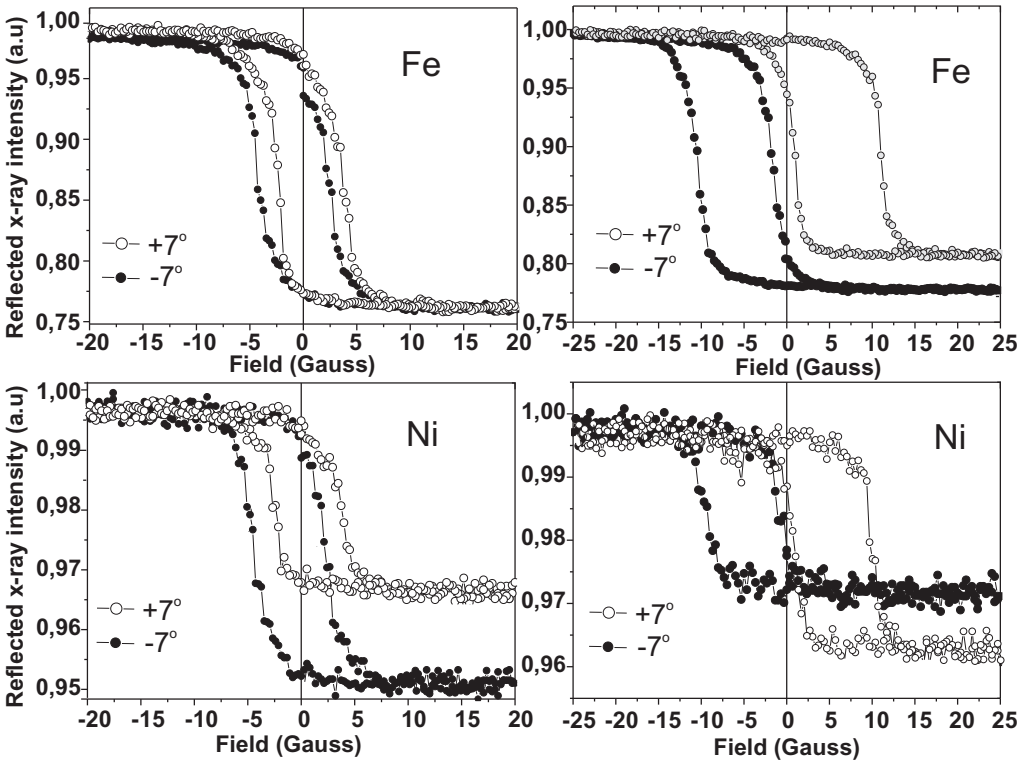

Figure 2. ESMH loops for the Fe edge (top) and Ni edge (bottom) at grazing incidence (+ and −7°). The loops for sample (a) with NiFe (5 nm)/FeMn (7 nm) are presented on the left-hand side and the loops for sample (b) with NiFe (5 nm)/FeMn (9 nm) are presented on the right-hand side. The two hysteresis loops in each of the panels were taken with the EB field direction parallel and anti-parallel to the incident x-rays (figure 1(c), measuring geometries 3 and 4).

exhibit a very small EB, which is found to be the same as the one obtained from standard magnetometry measurements based on the magneto-optical Kerr effect. When comparing the loops for the two samples in figure 2, we clearly observe Fe frozen moments in the case where the EB effect is stronger. No Fe frozen moments were detected with XMCD, in contrast to the case of Ni, a hint that frozen moments may contribute differently to the EB effect. Similar experiments were done for sample (b) and the result is presented in the right-hand side of figure 2. For the latter sample, we observe a larger horizontal shift of the hysteresis loops, i.e. a stronger EB. Moreover, we observe a vertical shift for both the Fe and Ni edges. We conclude that in this case the larger vertical ESMH shift, which is observed at the Ni edge for sample (a), does not correlate with the smaller EB effect, indicating that all frozen moments do not necessarily contribute equally to the EB effect.

For sample (a), we do not observe a normal XMCD signal for Fe and Mn in the TEY mode, but a small XMCD signal for Ni is evident. Interestingly, for samples (b) and (c) there is no XMCD for Fe, Mn and Ni when reversing the FM magnetization. As the thickness of the AFM layer on top of the FM layer increases, the corresponding electrons have a considerably reduced probability to escape, implying that we cannot probe sufficiently deep into the FM below the AFM when relying on the escaping electrons. In particular, we want to be sensitive to the

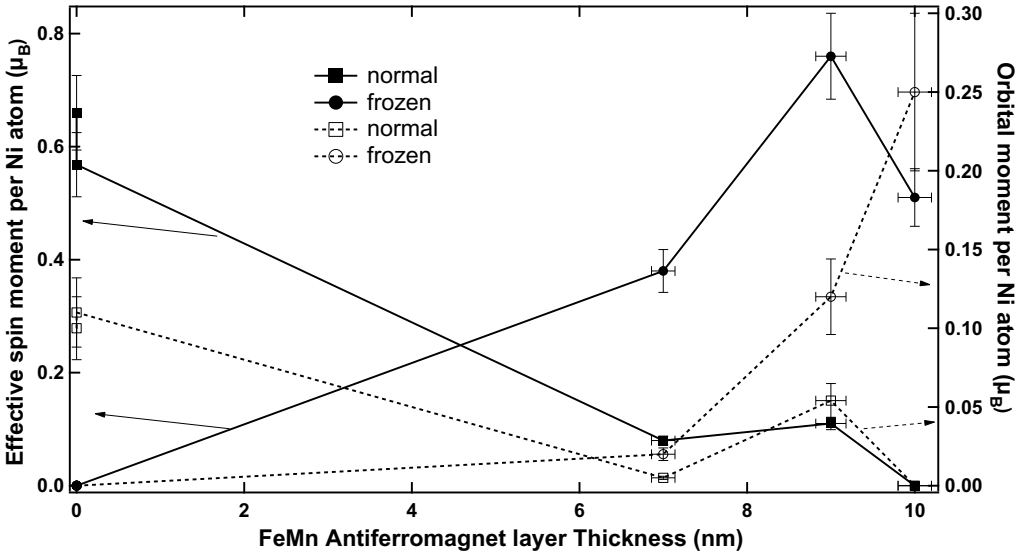

Figure 3. Results of the XMCD sum rules analysis for samples with NiFe/FeMn (7, 9 and 10 nm) and FeMn (0, 0, 7, 9 and 10 nm)/NiFe. The x-axis represents the FeMn overlayer thickness for the different samples measured. The thicker the FeMn overlayer the less the NiFe layer below is probed in depth by the electron yield technique. Closed and open symbols are for the spin and orbital moments, respectively. Rectangles are for the normal moments and circles are for frozen moments.

interface-specific frozen moments. Therefore, we combined the geometries 3 and 4 presented in figure 1(c). Applying this geometry we obtained an XMCD signal only for Ni. This signal can be linked to the interface area, where the spins are frozen and do not follow the FM magnetization.

The XMCD data were further analyzed by applying the XMCD sum rules [19, 20]. The obtained orbital and effective spin moments are presented in figure 3. The effective spin moment differs from the spin moment by the dipolar correction term, which is small for high-symmetry atomic environments [20]. The normalization of the x-ray absorption allows for the determination of the orbital and spin moments on a per atom basis [22, 23]. We are able to probe the Ni atoms of the NiFe layer through the FeMn layer and the 1.5 nm thick Au capping layer. The overall thickness of the layers (Au plus FeMn) implies that a damping factor should be taken into account for the Ni signal which is 70, 190 and 314 for samples (a)–(c), respectively. The corresponding Ni XMCD signal is small, but still clearly detectable. For a sample with the NiFe close to the free surface (sample (d)), we find that the spin moment obtained using the sum rule is close to the previously obtained value using the XMCD signal [24]. However, when compared to this previous study, we find an increase in Ni orbital moment. Given the particular thickness of the NiFe layer, such an effect can be traced back to a considerable increase of the Ni orbital moment on the FM side of the FM/AFM interface. Here, the XMCD signal for the frozen moment measurement geometries disappears within the noise; only the normal XMCD signal can be detected by reversing the NiFe magnetization. Any effect related to the interface should be more clearly seen when the FeMn layer is further away from the free sample surface. In this case the FM/AFM interface Ni atoms become more highlighted in the electron yield spectra because of the higher FeMn thickness. Hence a pure interface-specific frozen moment signal

may be detected. The results in figure 3 indeed indicate an increase of the orbital moment for the interface Ni atoms, in particular when relying on the frozen moment measurement geometries. As the thickness of the FeMn layer increases, a continuous decrease of the normal ferromagnetic signal is observed, reminiscent of the observation of moments localized at a surface or at an interface [22, 23]. The value of the effective spin moment indicates that in particular for sample (c) no normal XMCD can be detected. In this case the frozen moment XMCD signal reaches in magnitude the normal XMCD signal, implying that only frozen moments are probed. Our results point to a reduced symmetry environment for the corresponding Ni interface atoms, leading to an enhanced orbital moment contributing about 50% to the total magnetic moment. The strongest orbital moment value we obtain for the Ni atoms, in the case of the thickest 10 nm FeMn film, is 0.25 Bohr magnetons, a strong increase by a factor close to 4, as compared to the value of the orbital moment of Ni in permalloy films, of 0.06 Bohr magnetons. We therefore have a direct spectral signature of the so-called frozen moments at the FM/AFM interface. The increased orbital moment provides a natural way to explain how these frozen moments tie the FM magnetically to the AFM, i.e. by means of a strong spin–orbit interaction. This provides at least on the FM side localized electron scattering centers for a contribution that strongly ties the electronic degrees of freedom to the crystal lattice by means of the spin–orbit interaction [26]. For the data point in figure 3 for the sample with a FeMn thickness of 10 nm, the value of the effective spin moment is probably no longer fully representative of the value of the spin moment within the error bars, as a large value of the orbital moment may be indicative of a large lattice distortion, implying that the dipolar correction term needs to be taken into account.

We now turn to a comparison with other studies focusing on frozen magnetic moments. We found that there are only a few previous studies which relied on the use of x-rays. It was suggested by Ohldag *et al* [11] that the physical origin of EB is linked to a small fraction of uncompensated interfacial spins (about 4% of the interface layer) that are pinned to the AFM lattice and do not rotate in an external magnetic field. Ohldag *et al* have indicated the possibility to obtain a quantitative estimate of the EB field strength by introducing an effective interface and an effective exchange energy [11] for the Co/NiO, Co/IrMn and CoFe/PtMn systems. These were obtained by relying on the vertical shift of the hysteresis loops (see figure 2) taken in the TEY mode with a small probing depth (2 nm), similar to our XMCD experiments. Our hysteresis loops are taken in the XRR mode in order to obtain an improved signal-to-noise ratio. As indicated above, we hence probe down to a different depth (4–7 nm) below the surface. Both our XMCD and XRR data indicate that frozen moments are not necessarily localized in the immediate vicinity of the FM/AFM interface, but do extend about a monolayer into the FM. However, only a small fraction of those moments may carry an enhanced orbital moment that can link them to the macroscopic EB effect. The strength of the XMCD frozen moment signal is about 5% of the normal XMCD signal (see figures 1(a) and (b)), in good agreement with the earlier work of Ohldag *et al* [11] where 4% of a monolayer was obtained.

Tsunoda *et al* [17] found no vertical offset of the ESMH loops for CoFe/MnIr, in contrast to the results of Ohldag *et al* [11] for IrMn/Co. For our samples, we also detect a vertical shift of the ESMH loops. Interestingly, we cannot detect any dichroism at the Mn edges, in contrast to Tsunoda *et al* [17]. This may be related to the fact that the sequence of the layering at the FM/AFM interface for our samples is different from the samples of Tsunoda *et al.* Recently, Tang *et al* [25] suggested that interfacial uncompensated spins provide the net spin moments required for the EB in their NiFe/FeMn samples which were grown in the presence of higher magnetic fields. Tang *et al* proposed that the more interfacial uncompensated spins are

present, the larger the EB, in agreement with the fact that a thicker AFM results in a larger EB. Finally, Schmitz *et al* [28] have investigated the orbital moment of the Fe atoms in a Co/FeMn bilayer consisting of five atomic layers of Co on top of 12 atomic layers of FeMn. Schmitz *et al* found that the orbital moment of the Fe atoms in the AF layer reflects the unidirectional behavior of the EB effect in the biased state. They suggested that for their Co/FeMn bilayer the spin–orbit interaction acts between uncompensated spin moments which rotate with the FM and uncompensated orbital moments which are pinned by the anisotropy of the AFM.

In the present study, we combine the results on frozen magnetic moments probed down to two different depths by means of XMCD and XRR. The vertical shift of the hysteresis loops obtained from the XRR data (see figure 2) indicates the presence of frozen magnetic moments also away from the interface. On the one hand we obtain a larger number of frozen moments by means of XRR as these extend away from the FM/AFM interface. On the other hand, our XMCD results reveal that the orbital moment on the FM side of the FM/AFM interface is enhanced only for a small fraction of the uncompensated moments. Given the smaller escape depth of the electrons for our XMCD measurements, the Ni atoms of one or two layers away from the interface may have an enhanced orbital moment. In our XRR-based experiments several layers away from the interface are probed as well. The frozen moments closer to the FM/AFM interface correspond to the frozen moments that would cause a vertical shift of the ESMH hysteresis loops when these loops are taken in the TEY mode. We conclude that, most probably, the EB phenomenon on the FM side of the FM/AFM interface can be linked to moments with a strongly enhanced orbital moment.

We now turn to a rough estimate of the magneto-crystalline anisotropy (MCA) energy associated, within the FM, with the increase of the orbital moment which is measured on the FM side of the FM/AFM interface. When one tries to overcome the EB field and rotate the magnetization away from its easy direction, the corresponding MCA can be linked to the anisotropy of the orbital moment in the FM using a simple perturbative approach [26]. In the case of reorientation of the magnetic moments in thin FM films good quantitative results for the MCA were obtained based on the orbital moment anisotropy inferred from XMCD [26, 27]. The anisotropy of the orbital moment is closely related to the MCA energy ΔE_{so} resulting from the spin–orbit (SO) coupling when the magnetization direction is rotated away from the easy axis toward the hard axis (the hard axis is taken perpendicular to the easy axis). For a uni-axial anisotropy with the exchange splitting larger than the band width, this relation can, according to Bruno *et al* [26, 27], be expressed as

$$\Delta E_{\mathrm{so}} = E_{\mathrm{so}}^{\perp} - E_{\mathrm{so}}^{\parallel} = -\frac{G}{H}\frac{\xi}{4\mu_{\mathrm{B}}}\left(m_l^{\perp} - m_l^{\parallel}\right), \tag{1}$$

where the spin–orbit constant ξ is about 0.11 eV for Ni. The factor G/H, which is much smaller than unity, depends on the details of the electronic structure, and can be taken as equal to 0.2 [26, 27]. When applied to the FM side of the FM/AFM interface, this simple perturbative approach results for the magnetization rotation in an energy of about $10^3\ \mu$eV per frozen Ni atom for an orbital moment variation of $0.2\ \mu_{\mathrm{B}}$. The latter variation is in agreement with the variation of the magnetic moment presented in figure 3. Such an energy is about four orders of magnitude larger than the Zeeman energy associated with our characteristic EB field. Taking into account the large ratio between the MCA energy predicted by the Bruno *et al* equation on a per atom basis for a single frozen moment and the Zeeman energy of our EB field, we conclude that a single frozen moment provides sufficient energy to keep about 10^4 atoms fixed in the FM lattice.

The large ratio between the two energies is consistent with the small number of atoms that are found to carry a frozen moment and are located on the FM side of the FM/AFM interface (see figure 3). This confirms that the microscopic spin–orbit energy associated with very few frozen moments at the interface with low local symmetry atoms provides sufficient energy to account quantitatively for the macroscopic EB energy. With the XAS and XMCD techniques one probes predominantly the local electronic structure at the site of the photo-excited atom, implying that local information at the atomic level is obtained. Using the XMCD sum rules the local symmetry at the atomic level can be directly quantified in terms of atomic magnetic moments on a per atom basis. On the other hand, in the case of the XRR technique, where simulations are required, one probes the interface on a mesoscopic length scale, whose size depends on the transverse coherence of the x-ray beam.

The observation we make here, that spins characterized by their local symmetry to be in a frozen state versus the rest of the magnetization can either contribute to the macroscopic EB energy or not, opens up new opportunities for the understanding and exploitation of the EB effect at the atomic level. The theory covering the understanding of our observations starting from the atomic level measured here and leading to the macroscopic EB energy may not be simple. For such a description not only the electronic structure of the material may play a role, but also the existence of disorder. The XMCD results correlate the existence of EB to an enhanced orbital moment at the atomic level, and most probably, reduced lattice symmetry. The XRR technique, operating at a mesoscopic level, records also frozen spins and an EB effect as for macroscopic, inductive magnetization measurements. The combination of the XMCD and XRR techniques to track frozen spins establishes the length scale for an understanding of the EB effect, starting from first principles, to lie in the mesoscopic length range. Our results also open up the possibility for tailoring the EB effect at the atomic level, once such a description is achieved, based on the present work and on future measurements probing simultaneously the EB effect at different length scales.

In conclusion, for a NiFe/FeMn FM/AFM interface, we obtained evidence for the presence of both ‘passive’ and ‘active’ frozen magnetic moments on the FM side. To our knowledge, this is the first time that such a conclusion could be drawn from element-specific and interface-sensitive spectroscopies. Obviously, our results may inspire calculations which rely on the atomic spin–orbit energy to describe at the atomic level the type of interface distortion that best ties the magnetization of the FM to the AFM. This may result in establishing a reliable microscopic picture of the EB effect.

Acknowledgments

This work was supported by the European Community—Research Infrastructure Action under the FP6 ‘Structuring the European Research Area’ Programme (‘Integrating Activity on Synchrotron and Free Electron Laser Science’), the Swedish Research Council (VR), the Carl Tryggers Foundation for Scientific Research, as well as the Science Foundation—Flanders (FWO, Belgium) and the Flemish Concerted Action (GOA) and the Belgian Interuniversity Attraction Poles (IAP) research programs.

References

[1] Meiklejohn W H and Bean C P 1956 *Phys. Rev.* **102** 1413
[2] Meiklejohn W H and Bean C P 1957 *Phys. Rev.* **105** 904

[3] Nogués J and Schuller I K 1999 *J. Magn. Magn. Mater.* **192** 203
[4] Kools J C S 1996 *IEEE Trans. Magn.* **32** 3165
[5] Thompson D A and Best J S 2000 *IBM J. Res. Dev.* **44** 311
[6] Grochowski E and Hoyt R F 1996 *IEEE Trans. Magn.* **32** 1850
[7] Antel W J, Perjeru F and Harp G R 1999 *Phys. Rev. Lett.* **83** 1439
[8] Hase T P A *et al* 2001 *Appl. Phys. Lett.* **79** 985
[9] Ohldag H *et al* 2001 *Phys. Rev. Lett.* **87** 247201
[10] Roy S *et al* 2005 *Phys. Rev. Lett.* **95** 047201
Fitzsimmons M R *et al* 2007 *Superlatt. Microstruct.* **41** 109
[11] Ohldag H *et al* 2003 *Phys. Rev. Lett.* **91** 017203
[12] Takano K *et al* 1997 *Phys. Rev. Lett.* **79** 1130
[13] Kappenberger P *et al* 2003 *Phys. Rev. Lett.* **91** 267202
[14] Nogués J, Leighton C and Schuller I K 2000 *Phys. Rev.* B **61** 1315
[15] Mohanty J *et al* 2012 *Appl. Phys.* A **109** 181
[16] Ohldag H *et al* 2006 *Phys. Rev. Lett.* **96** 027203
[17] Tsunoda M *et al* 2006 *Appl. Phys. Lett.* **89** 172501
[18] Radu F *et al* 2006 *J. Magn. Magn. Mater.* **300** 206
[19] Thole B *et al* 1992 *Phys. Rev. Lett.* **68** 1943
[20] Carra P *et al* 1993 *Phys. Rev. Lett.* **70** 694
[21] Henke B L, Gullikson E M and Davis J C 1993 *At. Data Nucl. Data Tables* **54** 181
[22] Tischer M *et al* 1995 *Phys. Rev. Lett.* **75** 1602
[23] Samant M G *et al* 1994 *Phys. Rev. Lett.* **72** 1112
[24] Guan Y *et al* 2005 *J. Appl. Phys.* **97** 10A719
[25] Tang X-Li 2007 *J. Magn. Magn. Mater.* **312** 366
[26] Bruno P 1989 *Phys. Rev.* B **39** 865
[27] Weller D *et al* 1995 *Phys. Rev. Lett.* **75** 3752
[28] Schmitz D *et al* 2010 *Phys. Rev.* B **81** 224422